AN EXAMINATION OF ENGINE EFFECTS ON HELICOPTER AEROMECHANICS

David M. O'Brien, Jr., Mark E. Calvert, Steven L. Butler

Aviation Engineering Directorate
U.S. Army Research, Development and Engineering Command (RDECOM)
Redstone Arsenal, AL

David.OBrienJr@us.army.mil, Mark.E.Calvert@us.army.mil, Steven.L.Butler@us.army.mil

ABSTRACT

An engine modeling capability has been implemented into a Reynolds Averaged, Navier-Stokes based computational fluid dynamics code to assist in examining engine effects on helicopter aeromechanics. The procedure involves coupling a one-dimensional engine program to the flow solver through inlet and exhaust boundary conditions. Rotor influence is approximated with a time-averaged actuator disk model, which has a trim procedure capable of including fuselage loads. This simulation capability is found to provide useful insight for investigating aeromechanics problems that have been observed due to engine induced effects. In particular, this paper shows that this capability enables the visualization of the engine exhaust plume, provides estimates of the engine impact on helicopter trim, and assists in understanding the impact of various exhaust concepts.

NOTATION

A	Boundary surface area
a	Speed of sound
C	Matrix relating pilot controls to rotor pitch
C_P	Power coefficient, $P/\left(\rho\pi\,R^2\,V_{tip}^3\right)$
C_T	Thrust coefficient, $T/\left(\rho\pi\,R^2\,V_{tip}^2\right)$
$\vec{F}$	Force and moment target vector
$\vec{f}$	Force vector
J	Jacobian matrix
M	Mach number
$\dot{m}$	Mass flow rate, $\rho\,v\,\mathrm{A}$
N	Number of rotors
$\hat{n}$	Outward pointing unit normal vector
p	Static pressure
R	Tip radius or Specific gas constant
T	Temperature
$\hat{t}$	Exhaust direction unit vector
$\vec{U}_{pilot}$	Pilot control vector: collective stick, cyclic stick, pedal
$\vec{V}$	Velocity vector
v	Velocity scalar
Δ	Indicates an incremental value

γ	Ratio of specific heats, $\gamma = 1.4$
μ	Advance ratio, $\mu = V_\infty / V_{tip}$
$\vec{\theta}$	Rotor pitch vector, $\left\{\theta_0,\,\theta_{1S},\,\theta_{1C}\right\}^T$
ρ	Density
σ	Solidity, $Nc / \pi R$
$()_0$	Subscript for total or stagnation quantity

INTRODUCTION

Computational fluid dynamics (CFD) simulations frequently neglect engine induced effects on the aeromechanics of a rotary-wing vehicle. Naturally, the reason for this is that the capturing the aerodynamic influence of the rotor is a challenging problem without the complication of adding secondary influences. Another reason is that most CFD simulations are validated against wind-tunnel experiments, which rarely possess engines that are representative of a full-scale helicopter. However, modern helicopters utilize powerful engines, which can have a strong influence on the air flow near the inlet, exhaust, and beyond.

Many of the potential aerodynamic problems that are related to helicopter engines are known and have been documented in the literature. However, these problems can be difficult to predict a priori (i.e. while still in the design phase). One of the first issues faced when performing an engine / airframe integration effort is predicting the inlet conditions and the back pressure at the exhaust. These parameters regularly appear in a variety of equations for engine

performance predictions (see for example Ref. [1]). Due to the wide range of flight conditions experienced by a helicopter, the assumption of ambient values for the inlet and exhaust conditions may not always be sufficient.

Other issues, which are more difficult to predict, have also been observed. One example is the reingestion problem described in Ref. [2]. Although this particular reference refers to V/STOL aircraft like the Harrier or JSF, the reingestion problem has also been known to occur in helicopters. This problem occurs when hot exhaust flow recirculates back to the inlet, raising the inlet temperature and reducing the overall engine performance. Another difficulty occurs when comparing different engine exhaust configurations. Three IR suppressor concepts for the AH-1G tested in Ref. [3] where found to reduce hover capability by 140 to 200 lbs, increase level flight power required by 17 to 35 hp, and reduce maximum flight speed by 5 to 11 knots. Experimental efforts to improve IR suppressor concepts on the OH-58A (Ref. [4]) and AH-1G (Ref. [5]) could also have benefited from a CFD prediction capability.

Attempts to model external engine flow via CFD are not too common in the rotary wing field. The most common applications are found in fixed wing literature, see for example Refs. [6-8]. A CFD based engine plume simulation had been planned for the Comanche (Ref. [9]), but was never completed, since the program was cancelled. However, there have been a few efforts to model the external engine flow of a helicopter worth noting.

Le Chuiton (Ref. [10]) developed an engine plume simulation capability under the French-German program, Complete Helicopter AdvaNced Computational Environment (CHANCE). In this work, the engine is modeled through the use of an inlet and exhaust boundary condition, which conserves the mass flow rate. He observed that the exhaust plume impacted the horizontal tail and concluded that an analysis of the control surfaces needs to include the exhaust plume effects to obtain a reliable prediction of the loads on the tail.

Cao, et. al. (Ref. [11]) concentrated on simulating the flow near the engine inlet. This study focused on developing a capability to understand the potential for debris to enter the inlet in nap of the earth flight. Cao concluded that CFD methods can be used to gain insight into the potential for foreign object debris to enter the inlet and can assist in planning experiments.

While the works of Le Chuiton and Cao focus on simulating the engine induced flow field, this work concentrates on the engine flow effects on the vehicle aeromechanics. The first portion of this paper describes the current approach. The second part of

the paper examines a variety of test conditions to gain insight into the engine effects on aeromechanics problems.

NUMERICAL METHOD

The baseline method utilized in this work is the Reynolds Averaged Navier-Stokes (RANS) solver, FUN3D, developed by NASA Langley Research Center (Refs. [12-14]). FUN3D is an unstructured flow solver that uses a node-centered finite volume scheme. The solver is capable of second order accuracy in space and up to third order accuracy in time. All of the computations presented in this work are steady-state computations, so variable time stepping is used to speed up convergence.

Inviscid fluxes are computed with Roe's flux difference splitting scheme in this work, but other options are also available. Viscous fluxes are computed using a scheme similar to a central difference type formulation. The turbulence model can be either loosely or tightly coupled to the fluid equations and three different turbulence models are available: Spalart-Allmaras (SA), k-ω SST, and a SA detached eddy simulation (DES). In the present study only the loosely coupled SA model is exercised.

Rotor Model

In an effort to simplify the solution procedure the rotor is approximated as an actuator disk, which provides the rotor influence to the flow solver via source terms as proposed by Rajagopalan (Ref. [15]). The actuator disk model utilized in this work was developed under the HPC Institute for Advanced Rotor Modeling and Simulation (HI-ARMS) and is based on the previous work of O'Brien (Ref. [16]). Recent improvements under the HI-ARMS program include: a generalized blade description, airfoil tables, and a free-flight trim procedure capable of including multiple rotors and fuselage forces and moments.

The free-flight trim procedure is particularly relevant to the present work and requires further discussion. A typical actuator disk trim computation assumes a linear relationship between the rotor pitch angles and the target forces and moments. Any combination of forces and moments can be used in the target vector, but the typical set is the rotor thrust, pitching moment, and rolling moment. This approach is illustrated in the following equation:

$$\Delta \vec{\theta} = J^{-1}\left(\vec{F}_{\text{target}} - \vec{F}_{\text{rotor}}\right) \qquad (1)$$

The Jacobian matrix is determined by individually perturbing each of the control angles and measuring the affect on the rotor loads. By comparing the current loads on the rotor to the target loads it is

possible to estimate the incremental change to the rotor pitch angles to achieve the target loads. This type of trim procedure is useful for performing what is commonly referred to as wind-tunnel trim, but it does not effectively capture the coupling present in free-flight trim.

In a free-flight trim approach one must consider the ability to trim the entire aircraft (e.g. main rotor, tail rotor, and fuselage). The primary difference between the free-flight trim and the wind-tunnel trim procedure is the variables. The free-flight trim relates pilot controls to the target forces and moments as show below:

$$\Delta \vec{U}_{\text{pilot}} = J^{-1} \left(\vec{F}_{\text{target}} - \sum_{i=1}^{N} \vec{F}_{\text{rotor}}^{\,i} - \vec{F}_{\text{fuselage}} \right) \quad (2)$$

This equation is similar in form to Eq. 1, but includes additional force and moment contributions on the right hand side of the equation.

To complete the free-flight trim method the pilot controls need to be related to the blade pitch angles. Determining the blade angles will vary based on the system considered, but will have the following generalized form:

$$\begin{Bmatrix} \vec{\theta}^1 \\ \vdots \\ \vec{\theta}^N \end{Bmatrix} = C \, \vec{U}_{\text{pilot}} \quad (3)$$

The matrix relating the pilot controls to the rotor pitch angles is not necessarily a square matrix like the Jacobian in Eq. 1 and 2. For example, a tandem helicopter may have four pilot controls (pedal, collective, lateral, and longitudinal stick) and six rotor pitch angles (collective, lateral, and longitudinal pitch for each rotor), making C a 6 by 4 matrix.

Engine Model

Engine data is obtained by running a one-dimensional model provided by the manufacturer. This model is provided in the form of a computer program and follows the guidelines of MIL-E-8593A (Ref. [17]). The engine model provides data for each of the stages as well as information related to the overall engine performance over the operating envelop of the engine. However, only the inlet and exhaust states are relevant to the present work. In using the engine model properties, the assumption being made is that the flow is uniform over the engine boundary faces. Although this assumption is not true in reality, it is a sufficient approximation to obtain an initial estimate of the engine's influence on the external aerodynamics.

Another drawback of using the engine model is that it only provides data for the core engine flow.

Many designs include secondary cooling flow which must be included to obtain reliable solutions. If the geometry is well defined the secondary flows could be simulated directly. However, direct simulation may add an unnecessary amount of complexity to the problem, so the secondary flow is typically accounted for empirically when specifying the exhaust boundary condition.

Engine data is transferred to the flow solver through the use of engine inlet and engine exhaust boundary conditions. The principle of characteristics states that an outflow boundary will have four quantities determined from the interior flow, but will also require one condition to be specified from the exterior. The opposite is true at an inflow boundary, where four conditions must be specified and one is determined from the interior. A small degree of caution must be exercised when setting up the engine boundary conditions, since the naming convention contradicts initial intuition. For the external aerodynamics problem being studied in this work, the engine inlet is the outflow boundary and the engine exhaust is the inflow boundary. Both boundary conditions use mass flow as a specified quantity, but the exhaust boundary condition also specifies the flow direction and total temperature.

The engine inlet condition is patterned off of the condition used by Le Chuiton (Ref. [10]). Although the mass flow is nominally the specified quantity, the numerical condition is actually based on a specified static pressure. Therefore, the inlet condition is patterned off of a back pressure boundary condition. The static pressure is determined as a function of the current mass flow through the boundary as shown in Eq. 4.

$$p_{\text{B}}^{i+1} = p_{\text{B}}^{i} + 0.2 \left(\frac{\dot{m}_{\text{B}}^{i}}{\dot{m}_{\text{target}}} - 1 \right) \quad (4)$$

The relaxation factor of 0.2 has been observed to provide good convergence and stability. Larger values have a tendency to cause the inlet static pressure to exhibit large oscillations and smaller values were found to increase the number of iterations to convergence.

The primary difference between the condition used in this paper and the Le Chuiton condition is that Eq. 4 attempts to balance inlet mass flow with the target mass flow provided by the one-dimensional engine model whereas the Le Chuiton condition attempts to match the exhaust mass flow. Ideally the two approaches will be identical since conservation of mass dictates that the outflow should equal the inflow. However, engine losses and fuel injection can cause the inlet and exhaust mass flow rates to differ slightly. Additionally, the present approach was

selected to allow secondary flow to be included at the exhaust without having to include them at the inlet.

The engine exhaust boundary condition is based on the inflow boundary condition of Jirásek (Ref. [18]). The first step is to determine the exhaust velocity by assuming that the mass flow condition provides the velocity normal to the exhaust boundary face.

$$v_n = \frac{\dot{m}_{target}}{\rho\,A} \qquad (5)$$

The normal velocity provides the first component of the exhaust velocity vector. Using the specified direction of the exhaust velocity, the total velocity magnitude can be determined from the following relation.

$$v_{total} = \frac{v_n}{\hat{n} \bullet \hat{t}} \qquad (6)$$

Once the velocity magnitude is known, the exhaust direction vector can be utilized to specify the three components of velocity.

$$\vec{V}_{exhaust} = v_{total}\,\hat{t} \qquad (7)$$

Use of the exhaust direction vector provides flexibility in the definition of the exhaust boundary, but also introduces a degree of uncertainty if the average flow direction is not normal to the exhaust boundary face. When the flow direction is not normal to the boundary, the boundary area used in Eq. 5 may cause inaccurate predictions of the normal velocity.

The total temperature provides the fourth condition to complete the boundary condition. The first step is to determine the stagnation speed of sound.

$$a_0 = \sqrt{\gamma\,R\,T_0} \qquad (8)$$

The local speed of sound can then be determined through the use of isentropic relations.

$$a = \sqrt{a_0^2 - \frac{\gamma - 1}{2} v_{total}^2} \qquad (9)$$

Equation 9 enables the Mach number to be computed, which in turn provides the temperature through the following equation:

$$T = \frac{T_0}{1 + \frac{\gamma - 1}{2} M^2} \qquad (10)$$

Finally, the temperature is written in terms of density through application of the ideal gas law.

The final aspect of the engine boundary condition is to provide the loads generated by the engine. Loads are created through a combination of the pressure difference and momentum change at the inlet and exhaust. Following the example in Ref. [1]

the forces on the engine inlet and exhaust are given in the following equation:

$$\vec{f} = \left(p\,\hat{n} + \left(\vec{V} \bullet \hat{n} \right)\rho\,\vec{V} \right)A \qquad (11)$$

A quick inspection of Eq. 11 indicates that an inlet will produce a drag force, since the velocity dotted with the outward pointing normal is positive. An exhaust face will produce a thrust, since the velocity dotted with the outward pointing normal is negative.

Coupling Scheme

The first step of the process is to run the one-dimensional engine model for a given flight condition (i.e. altitude, temperature, and flight speed). This provides the initial condition for the engine boundary conditions in the flow solver. The CFD solution process can then begin. As flow is iteratively updated, the CFD solver passes the flow through the disk to the rotor module, which returns the rotor loading to the solver via source terms. At certain intervals the flow solver will pass fuselage loads to the rotor module's trim routine to enable a new set of trim controls to be computed via Eq. 2. Once the new trim state is computed, the power required is sent to the engine model to determine a new set of inlet and exhaust boundary conditions. This process continues until the solution converges. A diagram of the coupling scheme is shown in Fig. 1.
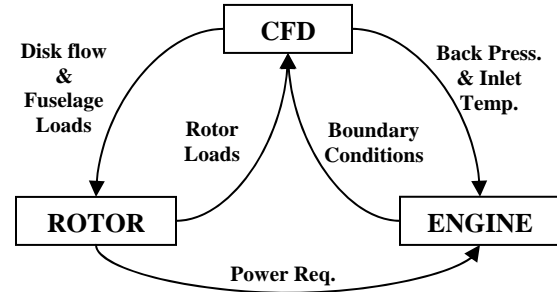

Figure 1. Diagram of the code coupling scheme.

RESULTS

Initial validation of the boundary condition involved comparing the CFD predicted quantities with inlet and exhaust conditions determined from a one-dimensional engine model. Although data from the engine model was used to specify the boundary conditions, it was important to ensure that other parameters that were not specified were consistent between the two. Good correlation was observed between the CFD simulation and the engine model, but can not be shown here, since the engine data is proprietary to the manufacturer.
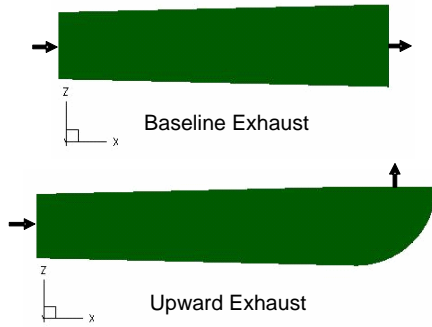
Figure 2. Side view of the engine configurations used in the initial simulation.

Initial Simulation

An initial simulation was performed to assess the ability of the engine model to assist in a theoretical trade study between two exhaust configurations. The baseline engine has a square cross-section at all stations. The alternative configuration has an upward exhaust similar to what was tried on the AH-1 (Refs. [3,5]). For simplicity the upward exhaust was generated by rotating the exhaust plane 90 degrees. Both engine configurations are depicted in Fig. 2.

A parametric study was performed on the baseline exhaust to study the influence of the exhaust total temperature on the computed engine loads. The results are summarized in Table 1. Drag is normalized by the inlet drag value at $T_0/T_{inf}=1$. The series of computations demonstrates that the exhaust temperature has little effect on the inlet drag and the nacelle drag. The exhaust produces a propulsive force in all cases which increases linearly as exhaust total temperature increases. The interesting aspect of this study is the effect on the total drag. For the two low temperature (i.e. "cold flow") cases the total drag is positive. As the exhaust temperature increases the drag becomes negative, indicating that the net engine force is a propulsive force.

A similar study was performed on the upward exhaust configuration and is summarized in Table 2. This configuration shows a small decrease in inlet drag compared to the baseline. Although small, the change in inlet drag can not be considered trivial, since the drag appears to be a function of exhaust temperature. As expected the exhaust face has virtually no influence on the drag, since this face is orthogonal to the direction of drag. However, it should be noted that the exhaust face does have a strong influence on lift. Compared to the baseline engine, the nacelle drag on the upward engine has increased substantially. The primary reason for this increase is the pressure force on the aft face of the configuration is now included in the nacelle (recall the aft face on the baseline engine is the exhaust face). As the exhaust temperature increases, the total drag on the upward exhaust engine is observed to increase. However, the effect of temperature is not as significant as it was with the baseline engine, since the exhaust temperature has the strongest influence on momentum based loads.

Table 1. Exhaust temperature effects on the drag of the baseline configuration normalized by baseline engine inlet drag at $T_0/T_{inf}=1$.

Exhaust T_0/T_{inf}	Normalized Inlet Drag	Normalized Exhaust Drag	Normalized Nacelle Drag	Normalized Total Drag
1.0	1.00	-0.77	0.05	0.28
1.5	1.00	-0.98	0.05	0.07
2.0	1.00	-1.23	0.05	-0.18
2.5	1.00	-1.49	0.05	-0.44
3.0	1.00	-1.76	0.05	-0.70

Table 2. Exhaust temperature effects on the drag of the upward configuration normalized by baseline engine inlet drag at $T_0/T_{inf}=1$.

Exhaust T_0/T_{inf}	Normalized Inlet Drag	Normalized Exhaust Drag	Normalized Nacelle Drag	Normalized Total Drag
1.0	0.98	0	0.91	1.90
1.5	0.98	0	1.01	1.99
2.0	0.97	0	1.07	2.04
2.5	0.96	0	1.11	2.06
3.0	0.95	0	1.12	2.07

Overall, the numbers in Table 1 and Table 2 highlight two important points:
- Exhaust temperature has a significant influence when evaluating engine forces.
- Total drag is influenced by momentum changes and aerodynamic effects.

Table 1 illustrates the importance of using the correct exhaust temperature. Although it is not as substantial for the upward exhaust drag, the exhaust temperature does have a strong influence on the lift generated by this configuration. The second point is demonstrated by a comparison of the two configurations. It is not sufficient to simply subtract the thrust generated by the baseline exhaust to predict the drag on the upward exhaust. At $T_0/T_{inf}=3$ this would lead to an estimated normalized drag of 1.05; however, the upward exhaust simulation predicts a normalized drag that is twice as large (i.e. 2.07). This can have a substantial impact on the total vehicle drag of many helicopters, which could cause a noticeable decrease in forward flight performance (e.g. the 5-11 knot reduction in maximum speed for the AH-1G in Ref. [3]).

A streamline comparison provides additional insight into the computed drag numbers. The streamlines for the two largest temperature cases are

shown in Fig. 3. The streamlines indicate that the straight exhaust integrates into the surrounding flow in a much cleaner manner than the upward exhaust. The upward exhaust disrupts the natural flow, making the engine appear larger than it actually is in the downstream wake.
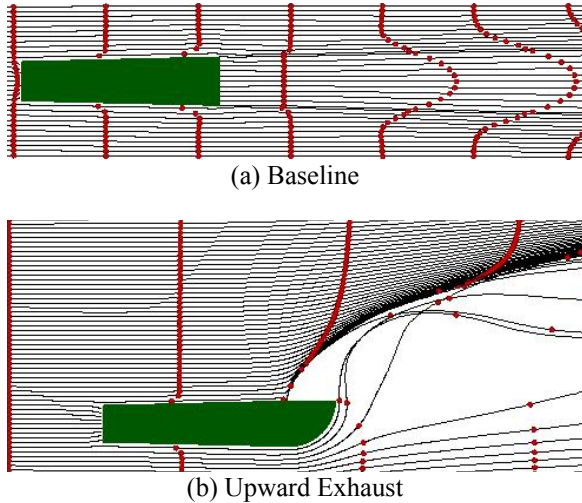

(a) Baseline

(b) Upward Exhaust

Figure 3.　Streamline comparisons for a baseline engine and an upward exhaust variant at an exhaust total temperature ratio of 3.

ROBIN Model

In an effort to study the effect of the engine on helicopter aeromechanics problems a more realistic configuration had to be utilized. The ROBIN model (Refs. [19,20]) served as the baseline geometry for this purpose. The rotor placement for this study is based on Ref. [19] (X/R=0.69, Y/R=0, Z/R=0.274) and the rotor shaft is tilted forward three degrees for all cases. For the purposes of this paper, the ROBIN nacelle was modified as show in Figs. 4 and 5. An inlet is placed on both the left and right side of the nacelle at the station, X/R = 0.7. The inlet is integrated into the nacelle by cutting a channel forward of the inlet face. The exhaust is modeled as an aft facing cylindrical pipe that is canted upward 10 degrees.

Three flight conditions were selected for this study: 20 KTAS, 70 KTAS, and 120 KTAS, representing a low, intermediate, and high speed case, respectively. Three rotor thrust loadings were selected from Ref. [20], C_T/σ = 0.040, 0.064, and 0.080. The geometry was scaled to a full size configuration by assuming a rotor radius of 15 ft and a rotation rate of 450 RPM. This leads to a rotor thrust of 3423 lb, 5477 lb, and 6847 lb for the three thrust loadings at sea level standard conditions. The three flight velocities correspond to advance ratios of

0.048, 0.167, and 0.286. Based on these parameters, the modified ROBIN model approximately equates to a scout helicopter configuration.

Two configurations are required to evaluate the impact of the engine model on the vehicle aeromechanics. Similar to the initial simulation, an upward exhaust was also added to the ROBIN configuration as shown in Fig. 6. The tailpipe was modified by rotating the aft face 80 degrees. Identical test conditions were selected for the upward exhaust configuration.
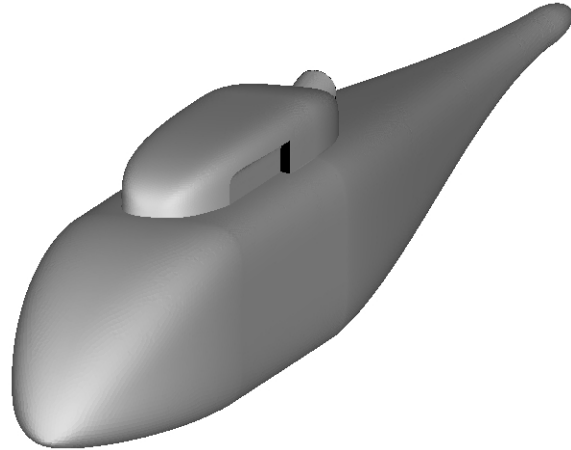

Figure 4.　ROBIN geometry with inlet and exhaust modification.

Figure 5.　Side view of the modified ROBIN nacelle with straight exhaust.

Figure 6.　Side view of the modified ROBIN nacelle with upward exhaust.

Since the ROBIN configuration does not possess an engine, no one-dimensional engine model was available for use in this study. Therefore, a hypothetical set of conditions was created for this engine. Each inlet was taken to have a mass flow rate of 3 lbm/s. The exhaust mass flow assumed a 30% increase in mass flow due to secondary flow, yielding a total mass flow of 7.8 lbm/s. The exhaust total temperature ratio was assumed to be 2.0. These engine conditions were applied to all nine test

conditions, but it should be noted that true engine conditions would be a function of the power required. In application of this method to a real problem the engine model would need to be provided with the rotor shaft power required to provide the appropriate numbers.

One of the first aeromechanics effects examined in this study was the implication of changing the exhaust angle as demonstrated in the initial simulation. The most prominent effect of changing the angle is the interaction of the jet with the local flow. This interaction is commonly referred to as a jet in cross-flow. One of the most noticeable features of a jet in cross-flow is development of a counter-rotating vortex pair. The initial development of this vortex pair is seen in the temperature contours shown in Fig. 7. As the vortex pair develops hot exhaust gas can be pulled around the edge of the exhaust duct. This effect is also illustrated in Fig. 8 taken from Ref. [5], where particles released inside the upstream edge of the exhaust duct are observed to remain attached to the outer shell of the duct.

In Figs 7 and 8 the exhaust flow is descending below the lip of the duct, which ultimately leads to an increase in temperature on the duct surface. Since the primary motivation for an upward facing exhaust system is to reduce IR characteristics of the helicopter, the heating of the duct is an unwanted characteristic. References [4] and [5] propose ways to improve an upward facing system by reducing the heating through the use of flow deflectors upstream of the exhaust.
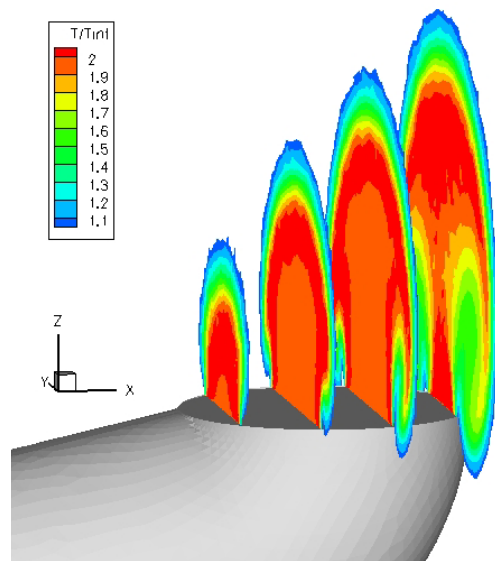

Figure 7.   Jet in cross-flow effect exhibited by the ROBIN upward exhaust at a high speed test condition: μ=0.287, C_T/σ =0.04.
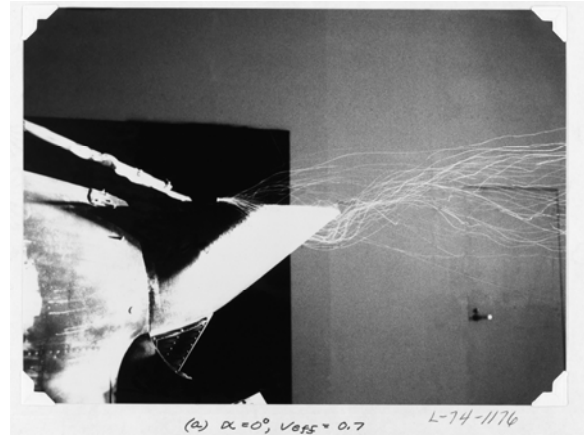

Figure 8.   Flow visualization showing the counter-rotating vortex effect. Taken from Ref. [5].

Another important aspect of implementing an engine model is the ability to visualize the exhaust plume to determine whether it will interact with other components on the vehicle. Figures 9, 10, and 11 show the exhaust plumes for low, intermediate, and high speed cases, respectively. The low speed case, shown in Fig. 9, illustrates the strong influence of the rotor wake. For the baseline exhaust the plume intersects the tailboom, indicating that caution would need to taken to ensure that temperature sensitive sensors were not placed in this area. The upward exhaust plume did not intersect the tailboom due to the counter-clockwise rotation of the rotor wake, but it does intersect the rotor disk. Intersection with the rotor disk can be problematic, since the high temperature exhaust is also a low density gas. This reduces the dynamic pressure of the air in the exhaust plume, which in turn can reduce the lifting capability of the rotor in these regions by 30% or more.

The intermediate flight speed, Fig. 10, begins to show characteristics of an increasingly influential freestream flow. The baseline exhaust plume is nearly straight at this condition. However, the two higher thrust loadings (not shown) do experience an increased influence of the rotor downwash. The upward exhaust plume is still observed to interact with the rotor disk at the intermediate flight speed, but the affected region of the rotor disk has decreased. The high speed test cases, Fig. 11, show little influence from the rotor wake. At the high speed condition the upward exhaust plume did not intersect the rotor disk.
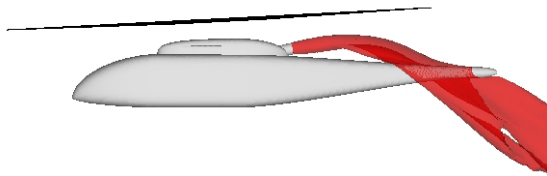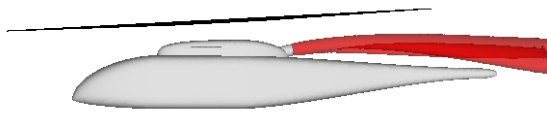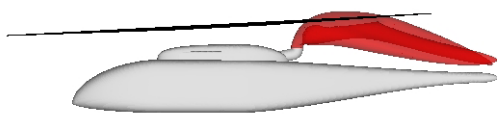
(a) Baseline Exhaust
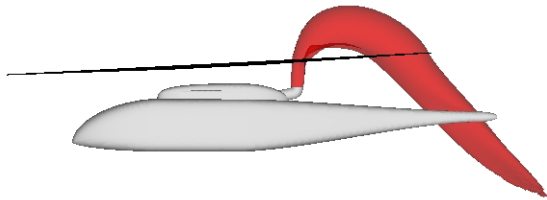
(b) Upward Exhaust

Figure 9. Exhaust plume comparison at a low speed, low thrust test condition: μ=0.048, C_T/σ =0.04.
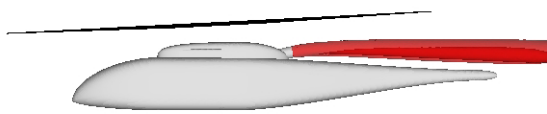

(a) Baseline Exhaust
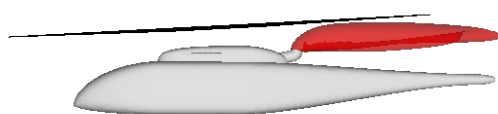

(b) Upward Exhaust

Figure 10. Exhaust plume comparison at the low speed, low thrust test condition: μ=0.167, C_T/σ =0.04.

(a) Baseline Exhaust

(b) Upward Exhaust

Figure 11. Exhaust plume comparison at a low speed, low thrust test condition: μ=0.287, C_T/σ =0.04.

Although visualization provides a useful tool, the significant aspect of this work is to evaluate the impact from a vehicle aeromechanics perspective. To appreciate this aspect the CFD fuselage and engine loads were coupled to the rotor trim routine as described earlier. In this respect, the thrust values from Ref. [20] were taken to represent the gross weight of the configuration. The rotor was then trimmed to balance the gross weight of the configuration and the fuselage download.

Figure 12 shows the resulting rotor thrust coefficients for the eighteen cases considered. Nominal thrust values are shown for comparison purposes. As expected the additional thrust required to balance the fuselage download is highest for the low speed cases. It is also seen that the high thrust case produces a larger delta from the nominal value than the low thrust case. All of the cases show that the upward exhaust increases the rotor thrust required to trim the aircraft.
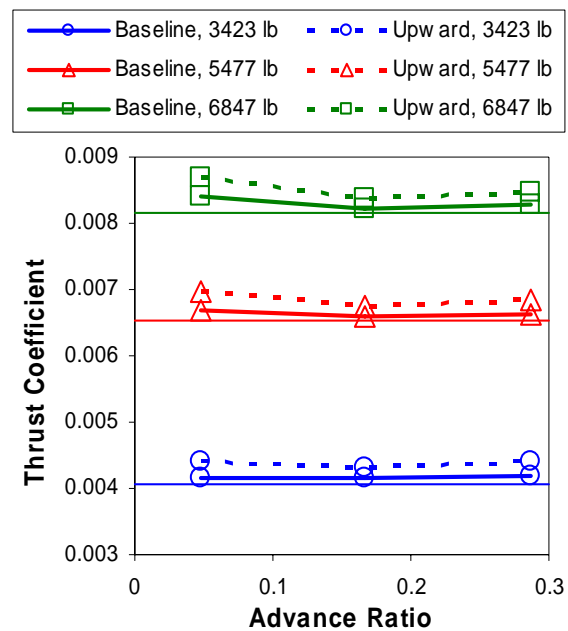

Figure 12. Influence of the fuselage loads on the rotor thrust computation.

Figure 13 shows the corresponding fuselage download. An interesting observation here is that the lowest download is found to occur at the intermediate flight speed for most of the cases. The reason for this is that this configuration has a negative lift coefficient at a zero degree angle of attack, which causes lift to decrease as velocity increases. However, as the influence of the rotor downwash becomes stronger, the download due the rotor dominates over the freestream value. Therefore, the low download for the intermediate flight speed is just

an indication that the freestream flow is the dominant factor for the intermediate and high speed cases and the rotor downwash is the dominant factor for the low speed cases.
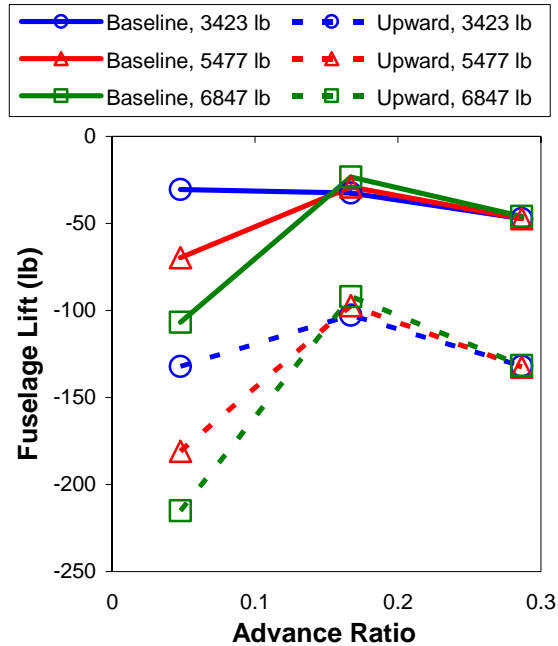

Figure 13. Variation of fuselage lift versus advance ratio for three gross weights.
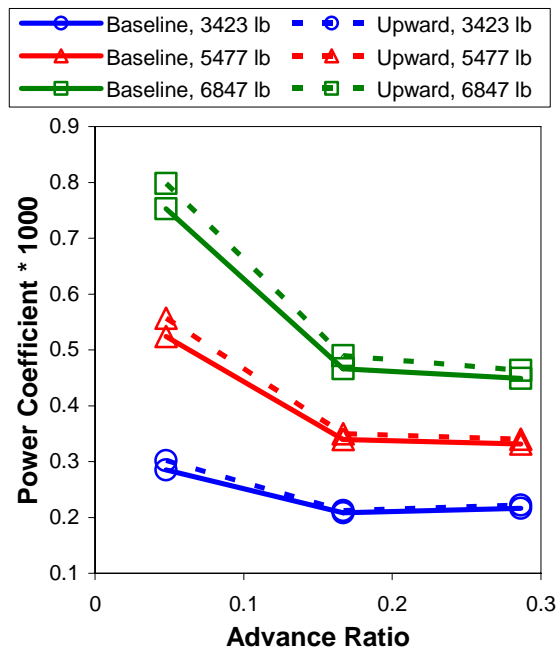

Figure 14. Power required for a variety of flight conditions.

The final aspect examined is the power required to operate the vehicle at these conditions. A plot of the power coefficient versus advance ratio is shown in Fig. 14. Typical trends are observed for both the standard and upward exhaust configurations. The upward exhaust requires more power for all nine conditions, but especially for the low speed case. The extra powered required for the upward exhaust is observed to increase as the power required for the baseline system increases. Therefore, it can be inferred from these results that the upward exhaust system would not have sufficient power to perform any operation that the baseline system can perform at maximum power.

It is interesting to note that the power required for the upward system was found to be less than the baseline if the fuselage and engine loads were not included in the rotor trim. This was observed in initial computations for these configurations that used the wind-tunnel trim approach.

CONCLUSIONS

An engine model has been coupled to a CFD code to develop a capability to simulate engine related effects. Key points from this work include

- Engine plume visualization can be used to identify potential interaction areas.
- Engine forces can have a significant impact on vehicle loads, especially when comparing alternative configurations.
- Vehicle forces and moments have a significant impact on the vehicle trim state.
- Exhaust modifications can have a significant impact on vehicle drag and power required.

ACKNOWLEDGEMENTS

REFERENCES

1. Hill, P., and Peterson, C., *Mechanics and Thermodynamics of Propulsion*, 2nd Edition, Addison-Wesley Publishing Company, New York, 1992.
2. Kirk, J., and Barrack, J., "Reingestion Characteristics and Inlet Flow Distortion of V/STOL Lift-Engine Fighter Characteristics," Journal of Aircraft, Vol. 6, (2), 1969.
3. Winn, A., and Stewart, R., "Performance and Handling Qualities Evaluation; AH-1G

Helicopter Equipped with Three Hot Metal/Plume Infrared Suppressors," USAAEFA Project No. 75-01, April 1975.

4. Shaw, C., and Wilson, J., "Wind-Tunnel Investigation of Simulated Engine Exhaust Interaction with Windstream," NASA TM X-3016, March 1974.

5. Wilson, J., and Mineck, R., "Wind-Tunnel Investigation of a Simulated Gunship Helicopter Engine-Exhaust – Windstream Interaction," NASA TM X-3161, December 1974.

6. Smith, C., and Podleski, S., "Comparison of F/A-18A Inlet Flow Analyses with Flight Data Part 1," Journal of Aircraft, Vol. 33, (3), 1996.

7. Rudnik, R., Rossow, C., and Geyr, H., "Numerical Simulation of Engine/Airframe Integration for High-Bypass Engines," Aerospace Science and Technology, Vol. 6, (1), 2002.

8. Pandya, S., Murman, S., and Aftosmis, M., "Validation of Inlet and Exhaust Boundary Conditions for a Cartesian Method," 22nd AIAA Applied Aerodynamics Conference, Providence, RI, August 2004.

9. Dimanlig, A., van Dam, C., and Duque, E., "Numerical Simulation of Helicopter Engine Plume in Forward Flight," NASA CR-197488, January 1994.

10. Le Chuiton, F., "Quasi-Steady Simulation of a Complete EC-145 Helicopter: Fuselage + Main/Tail Actuator Discs + Engines," 31st European Rotorcraft Forum, Florence, Italy, September 2005.

11. Cao, Y., Yuan, K., and Li, X., "Computational Methods for Simulation of Flow Around Helicopter Engine Inlet," Journal of Aircraft, Vol. 43, (1), January 2006, pp. 141-146.

12. Anderson, W., and Bonhaus, D., "An Implicit Upwind Algorithm for Computing Turbulent Flows on Unstructured Grids," Computers and Fluids, Vol. 23, (1), 1994, pp. 1-21.

13. Biedron, R., Vatsa, V., and Atkins, H., "Simulation of Unsteady Flows Using an Unstructured Navier-Stokes Solver on Moving and Stationary Grids," 23rd AIAA Applied Aerodynamics Conference, AIAA 2005-5093, Toronto, Canada, June 2005.

14. http://fun3d.larc.nasa.gov, "FUN3D Manual," Last visited November 30, 2007.

15. Rajagopalan, R., and Lim, C., "Laminar Flow Analysis of a Rotor in Hover," Journal of the American Helicopter Society, Vol. 36, (1), 1991, pp. 12-23.

16. O'Brien, D., *Analysis of Computational Modeling Techniques for Complete Rotorcraft Configurations*, Ph.D. Dissertation, Georgia Institute of Technology, May 2006.

17. "Engines, Aircraft, Turboshaft and Turboprop, General Specification For," MIL-E-8593A, October 15, 1975.

18. Jirasek, A., "Mass Flow Boundary Conditions for Subsonic Inflow and Outflow Boundary," AIAA Journal, Vol. 44, (5), May 2006, pp. 939-947.

19. Freeman, C., and Mineck, R., "Fuselage Surface Pressure Measurements of a Helicopter Wind-Tunnel Model with a 3.15 Meter Diameter Single Rotor," NASA TM 80051, March 1979.

20. Mineck, R., and Gorton, S., "Steady and Periodic Pressure Measurements on a Generic Helicopter Fuselage Model in the Presence of a Rotor," NASA TM 2000-210286, June 2000.